

## REFRACTIVITY FROM CLUTTER BY VARIATIONAL ADJOINT APPROACH

X.-F. Zhao and S.-X. Huang\*

Institute of Meteorology, PLA University of Science and Technology, Nanjing 211101, China

**Abstract**—Inferring refractivity profiles from radar sea clutter is a complex nonlinear optimization problem. Previous works treat this problem as a model parameter estimation issue by using some idealized refractivity models, such as the Log linear evaporation duct model, bilinear model, and trilinear model, to describe the synoptic structure of the real atmospheric conditions. However, these idealized models can not describe the exact information of the refractivity profile. Rather than estimating a few model parameters, this paper puts forward possibilities of retrieving the refractivity values at each point over height by variational adjoint approach for RFC measurement geometry. The adjoint model is derived from the parabolic equation method for a smooth, perfectly conducting surface and horizontal polarization conditions. Evaporation duct profiles collected at East China Sea are provided as the true refractive environment. The performance of this approach is determined via simulations and is evaluated as a function of: 1) the initial guess profile; 2) the measurement noise; and 3) the spatial samples.

### 1. INTRODUCTION

Nonstandard electromagnetic propagation due to formation of lower atmospheric sea duct is a common occurrence in maritime radar applications. Under this condition, some fundamental system parameters of seaborne radars can deviate significantly from their original values which are specified by the standard refractive conditions. These include extending the maximum operation range, creating radar ‘holes’, and increasing sea surface clutter. However, this unwanted clutter is a rich source of information about the atmospheric

---

*Received 16 June 2011, Accepted 20 July 2011, Scheduled 29 July 2011*

\* Corresponding author: Sixun Huang (huangxp@yahoo.com.cn).

environment and can be used to determine the local refractive conditions [1]. This technique is termed RFC, i.e., refractivity from clutter, which has the advantages of using radar itself as the remote sensing device and not needing additional hardware or extra meteorological or electromagnetic measurements.

RFC is a complex inverse problem because the relationship between refractivity values and radar sea clutter is clearly nonlinear and ill-posed. It is difficult to get analytical solutions according to current theories, and global optimization method might be a good choice to get approximate solutions [2]. Based on the experiments launched at Wallops Island (called Wallops98), many inversion procedures of RFC have been developed. *Tabrikian et al.* used a maximum a posteriori (MAP) approach to jointly estimate the refractivity and the spatially varying backscatter cross section [3]. *Rogers et al.* inferred evaporation duct heights on the basis of the assumptions of a range-independent environment and sea clutter radar cross section by a nonlinear least squares inversion procedure [4]. *Gerstoft et al.* proposed the usage of genetic algorithm (GA) to estimate refractivity. In their works, the authors presented a method to model the range and height varying refractivity of the environment using a total of 11 parameters [5], and some prior constraints were imposed to increase the accuracy of results over the coverage area of the radar [6]. *Barrios* utilized the rank correlation between the observed clutter power and the density of modeled ray paths to estimate surface-based duct parameters [7]. *Vasudevan et al.* exploited the inherent Markovian structure of the fast Fourier transform (FFT) to parabolic equation (PE) approximation and used a particle filtering approach to retrieve range-dependent atmospheric refractivity profiles [8]. *Yardim et al.* adopted Markov chain Monte Carlo (MCMC) sampling approach, a hybrid GA-MCMC method and Kalman Filters, respectively, to investigate RFC problem [9–11]. Through establishing many pre-computed, modeled radar clutter returns for different refractive environments in a database, *Douvenot et al.* inverted refractivity profiles based on finding the optimal environment from the database [12, 13]. Other researches on RFC techniques can be found in the literatures [14–16].

Instead of determining the refractivity at each point over height at a given range, all the methods mentioned above retrieve a few parameters to describe a probable characterization of the refractive index structure. The commonly used refractivity parameter models include the Log linear evaporation duct model, bilinear model, and trilinear model, see Fig. 1. However, using these idealized models can not describe the exact information of the refractivity profile. Some

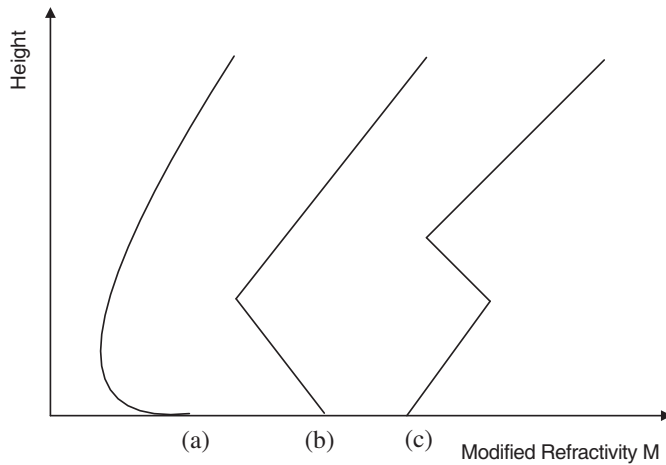


**Figure 1.** The three typical duct parameter models. (a) Log linear model. (b) Bilinear model. (c) Trilinear model.

small perturbations of the gradients of the refractivity profile are discarded, which might be duct structures. Another important issue of these methods is how to evaluate their performance under real time. Operational applications necessitate short computation time, less than ten minutes, to avoid error due to temporal evolution of refractivity [12]. Large numbers of the forward model runs make them impractical for real time operational use.

The adjoint method of control theory is known to give accurate and efficient data assimilation processes in oceanography and meteorology [17]. Using the adjoint of a forward propagation model has the potential to sharply reduce the number of modeling runs. Based on PE propagation model, the adjoint method has recently gained an increasing interest in the ocean acoustics community [18, 19]. In 2010, *Zhao et al.* have introduced this method into refractivity estimation problems, where the source-receiver configuration is assumed to be bistatic and the field measurements are observed from an array of radio receivers [20]. Making use of variational adjoint approach to retrieve the model parameters, in the process of solving the adjoint model, the terminal observation information can be placed on the adjoint initial or boundary conditions. This handling way has been adopted widely in atmospheric data assimilation problems [17]. When the measurements are observed within the computation domain, especially they are distributed along a horizontal line (similar to RFC measurement geometry), how to introduce the observation information into the adjoint model is a very trouble problem, which enhances the difficulty

of implementing the variational adjoint method. In the propagation problem, the observation information obtained from RFC measurement geometry can be introduced into the adjoint model by using Delta function. In general, when Delta function is involved in an equation, it is difficult to carry out numerical computations. Fortunately, an efficient method to solve the PE model is the split-step Fourier algorithm [21]. Making use of the solution to the forward model and the property of the Delta function integral, the adjoint model can also be solved by the split-step Fourier algorithm. The troublesome of Delta function can be successfully overcome by the Fourier integral.

In this paper, the adjoint approach for refractivity estimation is designed for RFC measurement geometry. The derivation of the adjoint model is accomplished by an analytical transformation of the governing differential equation, i.e., PE, in the continuous domain. After an exact gradient of the cost function is computed, the optimal solution of refractivity profile can be obtained by gradient-based iterations, which makes the computation real time. Rather than estimating a few refractivity parameters, the values of refractivity could be retrieved at each point over height, which is helpful to describe the vertical information of the refractivity in detail.

## 2. FORWARD MODEL

Before performing RFC estimations, a forward simulation of the received radar sea clutter power  $P_r$  has to be computed. Using the classical radar equation, the received radar sea clutter power  $P_r$  can be modeled as a function of the one-way propagation loss  $L_{loss}$  from the transmitter to the range cell, which in turn depends on the refractive environment  $\mathbf{m}$  in the troposphere [5]:

$$P_r(x, \mathbf{m}) = -2L_{loss}(x, \mathbf{m}) + 10 \log_{10}(x) + \sigma^0(x) + C \quad (1)$$

where  $\sigma^0(x)$  is the radar cross-section (RCS) of the sea surface at range  $x$ , and  $C$  is a constant that includes wavelength, transmitter power, antenna gain, etc.. If these values are known (how to compute the RCS accurately is a very difficult problem),  $P_r$  will be just determined by the propagation loss term  $L_{loss}$ , and  $L_{loss}$  can be computed as [22]:

$$L_{loss}(x, z) = -10 \log_{10} \left( \frac{\lambda^2 |u(x, z)|^2}{(4\pi)^2 x} \right) \quad (2)$$

where  $\lambda$  is the wavelength, and  $u$  is the electric field that can be computed numerically using the split-step Fourier PE method. For a smooth, perfectly conducting surface and horizontal polarization

conditions, the PE model can be described as such an initial value problem [23]:

$$\partial_z^2 u + 2ik_0 \partial_x u + k_0^2 (m^2 - 1) u = 0 \quad (3a)$$

$$u(x, 0) = 0 \quad (3b)$$

$$u(0, z) = \phi(z) \quad (3c)$$

where  $\partial_x \equiv \partial/\partial x$  and  $\partial_z \equiv \partial/\partial z$ .  $k_0$  is the free space wave number,  $m = m(x, z)$  is the modified index of refraction, takes into account the earth's curvature and is defined by  $m = n + z/a_e$ ,  $n$  being the index of refraction and  $a_e$  being the radius of the Earth.  $u(x, 0) = 0$  represents the boundary condition at  $z = 0$ , and  $u(0, z) = \phi(z)$  gives the initial field at the source range. In this paper, the transmitter simulates an omni-directional source. It is set at a height of 15 m and operating at a frequency of 2 GHz.

Let  $u(x_k, z)$  be the electric field at range  $x_k$  and height  $z$ . Then, the field at range  $x_{k+1}$  and height  $z$ , denoted by  $u(x_{k+1}, z)$ , can be given by the split-step Fourier solution to PE as [24]:

$$u(x_{k+1}, z) = \exp\left(i \frac{k_0}{2} (m^2 - 1) \delta x\right) F^{-1} \left\{ \exp\left(-i \frac{p^2 \delta x}{2k_0}\right) F[u(x_k, z)] \right\} \quad (4)$$

where  $F[\cdot]$  and  $F^{-1}[\cdot]$  are the Fourier transform and inverse Fourier transform, respectively.  $\delta x$  is the range increment, given by  $\delta x = x_{k+1} - x_k$ .  $p$  is the transform variable often referred to as the vertical wave number or spatial frequency. The Fourier transform pair is defined as:

$$U(x, p) = F[u(x, z)] = \int_{-Z}^Z u(x, z) \exp(-ipz) dz \quad (5)$$

$$u(x, z) = F^{-1}[U(x, p)] = \frac{1}{2\pi} \int_{-P}^P U(x, p) \exp(ipz) dp \quad (6)$$

Here, the transforms are written with limits of integration placed upon  $z$  and  $p$ , since the discrete Fourier transform, by way of the FFT, is actually used.  $Z$  and  $P$  can be determined by Nyquist's criteria:  $ZP = \pi N$ , where  $N$  is the transform size [25].

### 3. ADJOINT MODEL

As a theoretical investigation, the variational adjoint approach will be induced based on the following three assumptions.

- A. The spatial change of atmospheric refractivity is larger with height than with range and generally the range variations can be

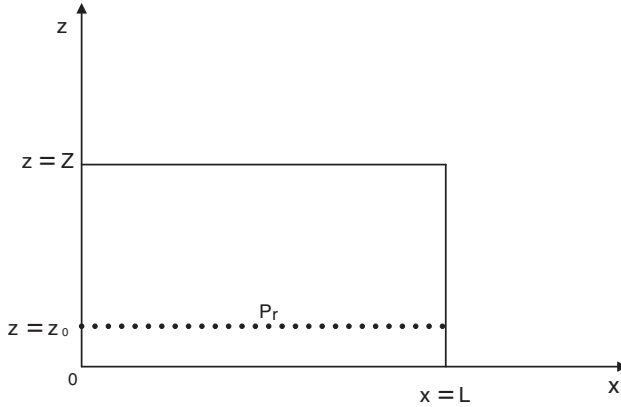


**Figure 2.** A drawing of the RFC measurement geometry.

neglected. In open ocean conditions, it was found that calculations of propagation enhancements based on a single profile were correct in 86 percent of the cases [26]. Therefore, the refractive conditions are considered laterally homogeneous, i.e.,  $m = m(z)$ .

- B. Using PE method, the field values at all range and height points can be obtained. However, the measured radar sea clutter power is only one value at each range. Hence, it is typically approximate the signal that is scattered at a given range from the PE field at a designated height  $z_0$  near the surface [9–11]. A drawing of the RFC measurement geometry is shown in Fig. 2.
- C. Since the real measured radar data are not available, for simplicity the electric field  $u$  is used to replace the radar sea clutter power  $P_r$  in our simulations. The relationship between  $P_r$  and  $u$  has been introduced in Section 2.

### 3.1. Tangent Linear Model

Set perturbations to  $m$  as:

$$\tilde{m}(z) = m(z) + \alpha \hat{m}(z) \quad (7)$$

where  $\hat{m}$  is the Gâteaux derivative of  $m$ :

$$\hat{m} = \lim_{\alpha \rightarrow 0} \frac{\tilde{m} - m}{\alpha} \quad (8)$$

Taking  $u$  and  $\tilde{u}$ , respectively, as the solution of the model (3) corresponding to  $m$  and  $\tilde{m}$ . Note  $\hat{u}(x, z)$  is the Gâteaux derivative of

$u(x, z)$ :

$$\hat{u} = \lim_{\alpha \rightarrow 0} \frac{\tilde{u} - u}{\alpha} \tag{9}$$

Then,  $\hat{u}$  satisfies the following tangent linear model:

$$\partial_z^2 \hat{u} + 2ik_0 \partial_x \hat{u} + k_0^2 (m^2 - 1) \hat{u} + 2k_0^2 um \hat{m} = 0 \tag{10a}$$

$$\hat{u}(0, z) = 0 \tag{10b}$$

$$\hat{u}(x, 0) = 0 \tag{10c}$$

### 3.2. Cost Function

Note  $u^{obs}(x, z_0)$  as the field measurement along the propagation distance  $L$ , and the field predicted by the forward model is noted as  $u(x, z_0)$ . Based on the standard matched field processing between a measured field and the corresponding predicted field, the simplest cost function  $J$  can be defined as:

$$J[m] = \frac{1}{2} \int_0^L |u(x, z_0) - u^{obs}(x, z_0)|^2 dx = \min! \tag{11}$$

Define two inner products as follows:

$$\langle f, h \rangle = \int_0^Z \int_0^L f \cdot \bar{h} dx dz \tag{12}$$

$$(f, h) = \int_0^Z f \cdot \bar{h} dz \tag{13}$$

where  $\bar{h}$  is the conjugate function of  $h$ .

The Gâteaux derivative of  $J[m]$  with respect to  $\hat{m}$  at point  $m$  is:

$$\begin{aligned} J'[m; \hat{m}] &= \lim_{\alpha \rightarrow 0} \frac{J[\tilde{m}] - J[m]}{\alpha} \\ &= \frac{1}{2} \lim_{\alpha \rightarrow 0} \frac{\int_0^L \left( |\tilde{u}(x, z_0) - u^{obs}(x, z_0)|^2 - |u(x, z_0) - u^{obs}(x, z_0)|^2 \right) dx}{\alpha} \\ &= \text{Re} \left[ \int_0^L \left( u(x, z_0) - u^{obs}(x, z_0) \right) \cdot \bar{\hat{u}}(x, z_0) dx \right] \end{aligned} \tag{14}$$

where  $\text{Re}[u]$  is the real component of a complex variable  $u$ .

On the other hand, from the definition of  $J'[m; \hat{m}]$ :

$$J'[m; \hat{m}] \equiv (\nabla_m J, \hat{m}) \tag{15}$$

Combining Eq. (14) with Eq. (15), the following equation can be obtained:

$$\text{Re} \left[ \int_0^L \left( u(x, z_0) - u^{obs}(x, z_0) \right) \cdot \bar{\hat{u}}(x, z_0) dx \right] = (\nabla_m J, \hat{m}) \tag{16}$$

### 3.3. Adjoint Model

The adjoint model can be obtained from the tangent linear model. Multiply the conjugate of Eq. (10a) by the adjoint field  $w(x, z)$ , and then integrate it on the domain  $[0, L] \times [0, Z]$ :

$$\langle w, \partial_z^2 \hat{u} \rangle + \langle w, 2ik_0 \partial_x \hat{u} \rangle + \langle w, k_0^2 (m^2 - 1) \hat{u} \rangle + \langle w, 2k_0^2 um \hat{m} \rangle = 0 \quad (17)$$

where

$$\begin{aligned} \langle w, \partial_z^2 \hat{u} \rangle &= \int_0^Z \int_0^L w \cdot \partial_z^2 \bar{u} \, dx dz \\ &= \int_0^L \left( w \cdot \partial_z \bar{u} - \partial_z w \cdot \bar{u} \Big|_{z=0}^{z=Z} \right) dx + \langle \partial_z^2 w, \hat{u} \rangle \end{aligned} \quad (18)$$

$$\begin{aligned} \langle w, 2ik_0 \partial_x \hat{u} \rangle &= \int_0^Z \int_0^L (-2ik_0 w \cdot \partial_x \bar{u}) \, dx dz \\ &= \langle 2ik_0 \partial_x w, \hat{u} \rangle - \int_0^Z \left( 2ik_0 w \cdot \bar{u} \Big|_{x=0}^{x=L} \right) dz \end{aligned} \quad (19)$$

$$\begin{aligned} \langle w, k_0^2 (m^2 - 1) \hat{u} \rangle &= \int_0^Z \int_0^L k_0^2 (m^2 - 1) \cdot w \cdot \bar{u} \, dx dz \\ &= \langle k_0^2 (m^2 - 1) w, \hat{u} \rangle \end{aligned} \quad (20)$$

$$\begin{aligned} \langle w, 2k_0^2 um \hat{m} \rangle &= \int_0^Z \int_0^L 2k_0^2 \cdot m \cdot \hat{m} \cdot \bar{u} \cdot w \, dx dz \\ &= \langle 2k_0^2 m \bar{u} w, \hat{m} \rangle \end{aligned} \quad (21)$$

Substitute Eqs. (18)–(21) into Eq. (17) to obtain:

$$\begin{aligned} &\langle \partial_z^2 w + 2ik_0 \partial_x w + k_0^2 (m^2 - 1) w, \hat{u} \rangle + \langle 2k_0^2 m \bar{u} w, \hat{m} \rangle \\ &+ \int_0^L \left( w \cdot \partial_z \bar{u} - \partial_z w \cdot \bar{u} \Big|_{z=0}^{z=Z} \right) dx - \int_0^Z \left( 2ik_0 w \cdot \bar{u} \Big|_{x=0}^{x=L} \right) dz = 0 \end{aligned} \quad (22)$$

Referring to the initial boundary conditions of the tangent linear model, the conjugate initial boundary conditions of the adjoint field can be set as  $w(x, 0) = 0$ ,  $w(x, Z) = 0$ , and  $w(L, z) = 0$ . Then, Eq. (22) can be reduced to:

$$\langle \partial_z^2 w + 2ik_0 \partial_x w + k_0^2 (m^2 - 1) w, \hat{u} \rangle = - \langle 2k_0^2 m \bar{u} w, \hat{m} \rangle \quad (23)$$

Next, how to introduce the observation information into the adjoint model is the most important problem. From the above derivation, the observation data are contained in Eq. (16), but they are just distributed along a horizontal line at height  $z_0$ . Comparing

Eq. (16) with Eq. (23), we could use Delta function to modify the left side of Eq. (16) as:

$$\begin{aligned} & \operatorname{Re} \left[ \int_0^L \left( u(x, z_0) - u^{obs}(x, z_0) \right) \cdot \tilde{u}(x, z_0) dx \right] \\ &= \operatorname{Re} \left[ \int_0^Z \int_0^L \left( u(x, z) - u^{obs}(x, z) \right) \cdot \tilde{u}(x, z) \cdot \delta(z - z_0) dx dz \right] \\ &= \operatorname{Re} \left[ \left\langle \left( u(x, z) - u^{obs}(x, z) \right) \delta(z - z_0), \hat{u}(x, z) \right\rangle \right] \end{aligned} \quad (24)$$

Then, Eq. (16) can be written as:

$$\operatorname{Re} \left[ \left\langle \left( u(x, z) - u^{obs}(x, z) \right) \delta(z - z_0), \hat{u}(x, z) \right\rangle \right] = (\nabla_m J, \hat{m}) \quad (25)$$

Take the real component of both side of Eq. (23):

$$\operatorname{Re} \left[ \left\langle \partial_z^2 w + 2ik_0 \partial_x w + k_0^2 (m^2 - 1) w, \hat{u} \right\rangle \right] = -\operatorname{Re} \left[ \left\langle 2k_0^2 m \bar{u} w, \hat{m} \right\rangle \right] \quad (26)$$

Let the left side and right side of Eq. (25) equal to the left side and right side of Eq. (26), respectively. Then, the following adjoint equation and the corresponding initial boundary conditions can be obtained as:

$$\partial_z^2 w + 2ik_0 \partial_x w + k_0^2 (m^2 - 1) w = \left[ u(x, z) - u^{obs}(x, z) \right] \delta(z - z_0) \quad (27a)$$

$$w(x, 0) = 0 \quad (27b)$$

$$w(L, z) = 0 \quad (27c)$$

Simultaneously, the gradient of the cost function  $J$  at point  $m$  can be obtained as:

$$\nabla_m J = -2k_0^2 m \int_0^L \operatorname{Re} [\bar{u} \cdot w] dx \quad (28)$$

With the gradient of the cost function, minimization could be generally accomplished through the use of standard iterative gradient-based methods:

$$m^{i+1} = m^i - \nabla_m J |_{m^i} \cdot \rho_i \quad (29)$$

In this paper, an efficient quasi-Newton gradient technique (L-BFGS-B) for large-scale bound constrained optimization is used for this purpose, where  $\rho_i$  is a good approximation to the inverse Hessian matrix [27].

### 3.4. Solution of the Adjoint Model

From Eq. (28), the exact gradient information depends on the solutions of the forward model (3) and the adjoint model (27). Making use of the

solution to the forward model and the property of the Delta function integral, the adjoint model can also be solved by the split-step Fourier algorithm:

$$W(x_k, p) = \exp \left\{ \frac{k_0^2(m^2 - 1) - p^2}{2ik_0} \delta x \right\} \cdot W(x_{k+1}, p) + \frac{1}{2ik_0} \int_{x_{k+1}}^{x_k} G(x, p) \cdot \exp \left\{ \frac{k_0^2(m^2 - 1) - p^2}{2ik_0} (x - x_k) \right\} dx \quad (30)$$

and

$$w(x_k, z) = F^{-1}[W(x_k, p)] \quad (31)$$

where  $\delta x$  is the range increment, given by  $\delta x = x_{k+1} - x_k$ , which should be identical to the range increment  $\delta x$  given in Eq. (4). However, being different from the solution of Eq. (4),  $w(x_k, z)$  is obtained by integrating the adjoint model in the reverse direction.  $G(x, p)$  is the Fourier transform of  $g(x, z)$ , where

$$g(x, z) = [u(x, z) - u^{obs}(x, z)] \delta(z - z_0) \quad (32)$$

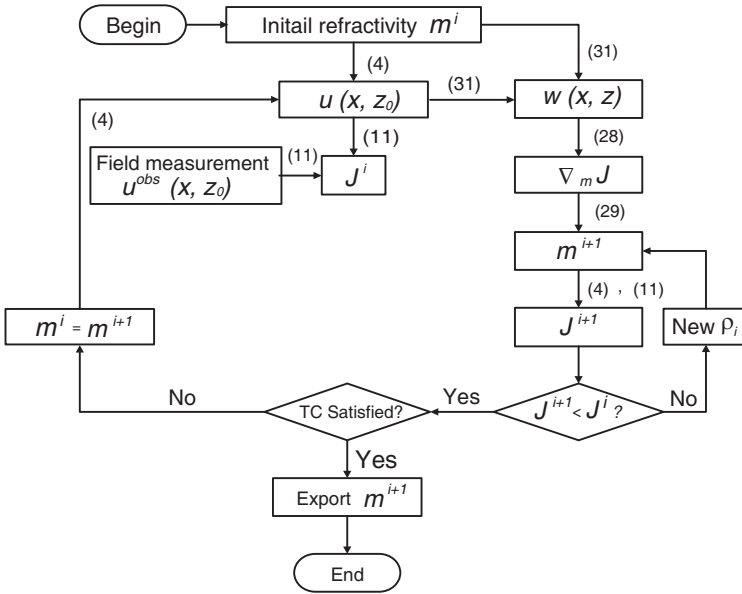


Figure 3. Scheme of iteration process.

and

$$\begin{aligned}
 G(x, p) &= F[g(x, z)] \\
 &= \int_{-Z}^Z [u(x, z) - u^{obs}(x, z)] \delta(z - z_0) \exp(-ipz) dz \\
 &= [u(x, z_0) - u^{obs}(x, z_0)] \exp(-ipz_0)
 \end{aligned} \tag{33}$$

Here, it should be noted that the forward and inverse Fourier transforms defined by Eq. (5) and Eq. (6) are written in continuous forms, but with limits of integration placed upon  $z$  and  $p$ . An abrupt truncation of the field in height will result in strong reflections from the nonphysical upper boundary. A practical approach to this problem is to add an ‘absorbing’ region above the maximum altitude of interest where the field is attenuated smoothly to zero at height  $Z$  [24]. Here, a cosine-tapered (Tukey) filter array [28] is used to filter the upper 1/4 of the field for this purpose.

The whole iteration process can be expressed as a flowchart in Fig. 3, where ‘TC (termination condition) satisfied?’ means as long as one of the following conditions are satisfied, the program will stop: 1) the cost function is less than a pre-given small positive number; 2) the gradient of the cost function approaches to zero; 3) the value of the cost function no longer descends; and 4) the maximum iteration number achieves.

#### 4. NUMERICAL EXPERIMENTS AND ANALYSIS

Since the radar measured data are not available, numerical experiments will be performed to test the theoretical results above.

In the propagation assessment, a quantity frequently used to describe atmospheric refractive conditions is the modified refractivity  $M$ , which is related to the modified index of refraction as follows:

$$M = 10^6 \times (m - 1) \tag{34}$$

In our simulations, an evaporation duct profile measured by low altitude captive balloon at East China Sea is used to model as the observed modified refractivity profile (see Fig. 4), and the corresponding electric field at height 1 m computed by the split-step Fourier PE propagation model is used as the observed radar data. The transmitter simulating an omni-directional source operating at 2 GHz is set at a height of 15 m. In the implementation of the fast Fourier transform, the transform size  $N$  is set to be the order of 64 to satisfy  $N = 2^6$ , and the vertical increment in  $z$ -space is set to be 1 m.

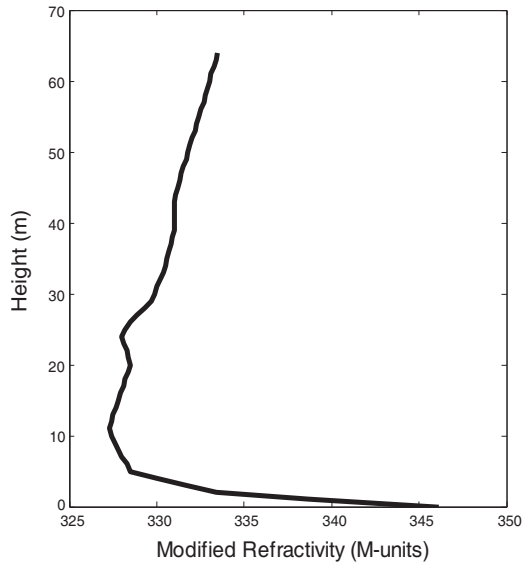


**Figure 4.** The observed modified refractivity profile.

The performance of the inversions is evaluated as a function of: 1) the initial guess profile; 2) the measurement noise; and 3) the spatial samples.

#### 4.1. Influence of the initial guess profile

The adjoint process is a local optimization method and the initial guess has an impact on the inversion accuracy. If the initial guess is too far from the correct solution, there is no mechanism for escaping a spurious local minimum [18].

Three initial guess profiles are selected in this section. The first is a linear profile with the typical gradient of 0.118 M-units/m and the M value of 350 M-units at sea level. The second is a linear profile with M value of 330 M-units at sea level. The third is a statistical result from the hydrometeorological data collected at East China Sea [29], which is constructed using the Log linear evaporation duct formula given by *Hitney and Vieth* [30] with an evaporation duct height of 9.1 m and the M value of 339 M-units at sea level. Fig. 5 to Fig. 7 give the retrieved results of the above three different initial guess profiles, where the observed profile is shown as real line, the initial guess profile is shown as dashed line, and the retrieved profile is shown as dotted line. The left and the right subplots show the results for different iteration numbers. A single iteration process consists of using

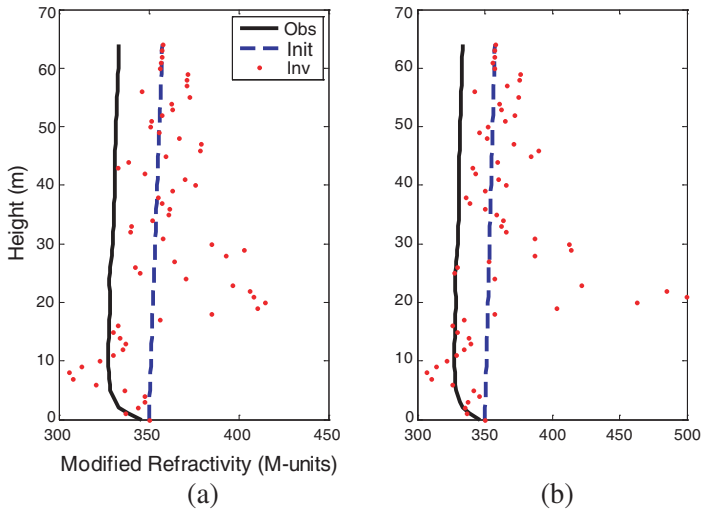


**Figure 5.** Inversions for a linear initial guess profile with the typical gradient of 0.118 M-units/m and the M value of 350 M-units at sea level. (a) 100 iteration numbers. (b) 2153 iteration numbers.

the forward model to calculate a modeled electric field, and then using the adjoint model to calculate a corrected refractivity profile. Here, the propagation distance is 50 km, the range increment  $\delta x$  is 20 m, and the constrained M value boundary is from 250 to 500 M-units.

From the above three Figures, it is clear that: 1) rather than retrieving several refractivity model parameters, the adjoint approach could retrieve the refractivity values at each point over height; 2) the whole retrievals for Fig. 5 are corrupt. This is because the initial guess profile for Fig. 5 is far from the true profile. Owing to the value of the cost function no longer descends, the program terminated at 2153 iteration numbers. Compared Fig. 5(a) with Fig. 5(b), the retrieved results of 2153 iteration numbers is similar to that of 100 iteration numbers, which means that the retrievals have trapped into a spurious local minimum; 3) the retrieved values above 50 m are poor. The reason of this phenomenon is that using the fast Fourier transform, the upper 1/4 field is filtered by the Tukey array; 4) the refractivity at sea level is equal to the value of the initial profile. This is because the lower boundaries of the forward and adjoint models are fixed to zero; 5) when the initial guess profiles are fairish, different initial guess profile requires different iteration numbers to get the optimal result. Compared Fig. 6 with Fig. 7, at 100 iteration numbers, giving a better initial profile could improve the inversions to some extent.

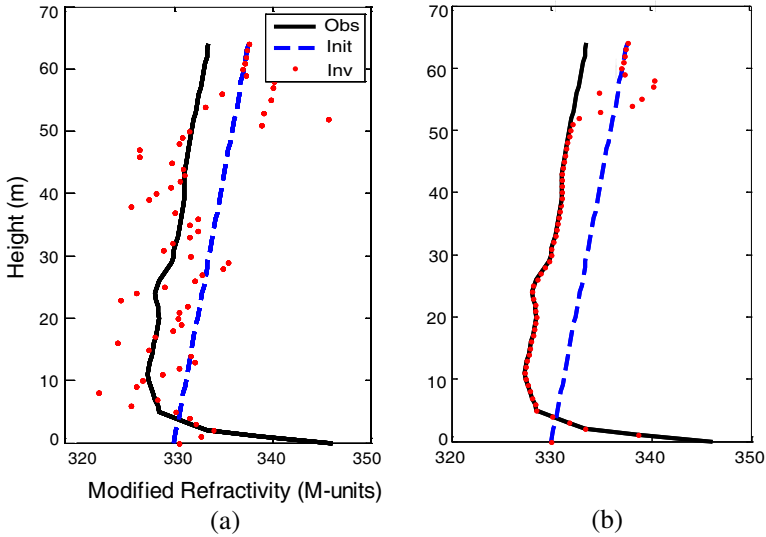


**Figure 6.** Inversions for a linear initial guess profile with the typical gradient of 0.118 M-units/m and the M value of 330 M-units at sea level. (a) 100 iteration numbers. (b) 400 iteration numbers.

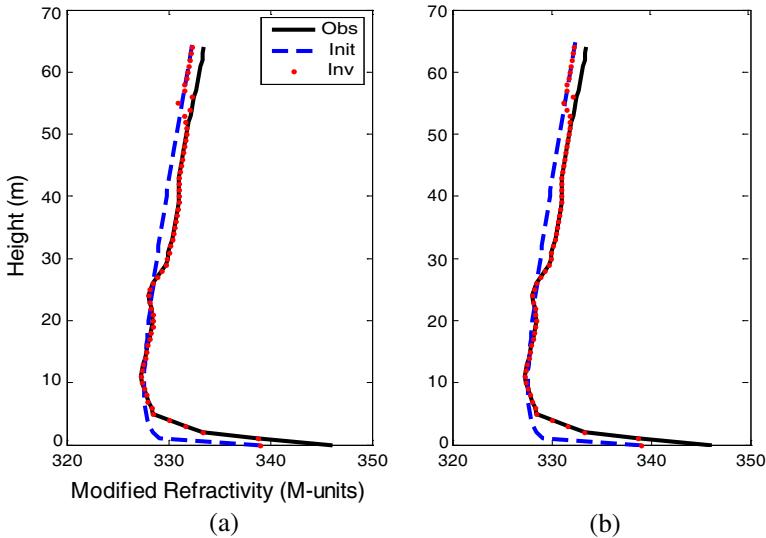


**Figure 7.** Inversions for a Log linear initial guess profile. (a) 100 iteration numbers. (b) 400 iteration numbers.

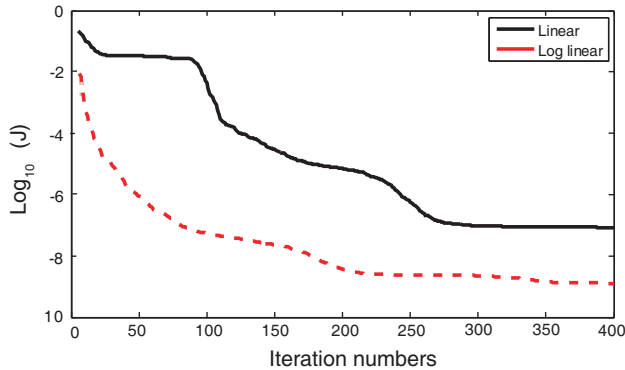


**Figure 8.** Evolution of the cost function produced by each iterative process.

Figure 8 shows the base-ten logarithm of the cost function  $J$  at iterations 1-400 for the latter two initial guess profiles. The black is for the linear profile with gradient of 0.118 M-units/m and the M value of 330 M-units at sea level. The red dashed line is for the Log linear evaporation duct profile.

It is clear that the decreasing of the cost function produced by the Log linear initial guess profile is faster than that produced by the linear profile. However, when the inversion accuracy achieves to some extent, the cost functions will decrease smoothly. In general, a favorable initial guess profile can always be obtained from history observations and/or from the output of numerical weather prediction model. Therefore, in the following computations, only Log linear initial guess profile will be considered and the maximum iteration number is set to be 400 (In Gerstoft et al.'s paper, the number of the forward model runs is 20000 [5], and Yardim et al.'s work requires more number of the model runs [9]). By the way, with 400 iteration numbers, the computation time is just approximate to 37.5seconds. Our computation source is ThinkPad R400 equipping with dual CPUs (P8600, 2.40 GHz) and 2 GB EMS memory bank.

#### 4.2. Influence of the Measurement Noise

In practical operations, the available measurements are often contaminated by some noise. Here, 10% and 20% additive white Gaussian noise are added to the measured field to investigate the anti-noise ability of the variational adjoint approach for RFC inversions. The propagation distance is 50 km, and the range increment  $\delta x$  is 20 m. Owing to the value of the cost function no longer descends,

in 10% Gaussian noise case, the program terminated at 249 iterations. While in 20% case, the program terminated at 232 iterations. Fig. 9 gives the retrieved profiles with the above two different additive noises.

Owing to the Gaussian noise added to measurements, the inversions become ill-posed. The higher the Gaussian noise is added, the larger intervals will be apart from the true values. However, the retrievals fluctuate surrounding the observed profile. Previous studies of the inverse problem have indicated that regularization technique might be a good tool to deal with these ill-posed problems and make the inversions stable [17]. However, several regularization terms, including H1 mode and L2 mode, have been tried in this problem, but no one has prominent improvement. H1 mode and L2 mode can be expressed as [31]:

$$H^1 = \left\{ u \left| \int_0^Z \int_0^L (|u|^2 + |\partial u / \partial z|^2) dx dz < +\infty \right. \right\} \quad (35)$$

$$L^2 = \left\{ u \left| \int_0^Z \int_0^L |u|^2 dx dz < +\infty \right. \right\} \quad (36)$$

In this paper, an alternative moving average filter called curve fitting method is adopted. This filter can be realized by ‘smooth’ function in Matlab. Fig. 10 gives the filtered profile of the above inversions (the value at sea level is not included).

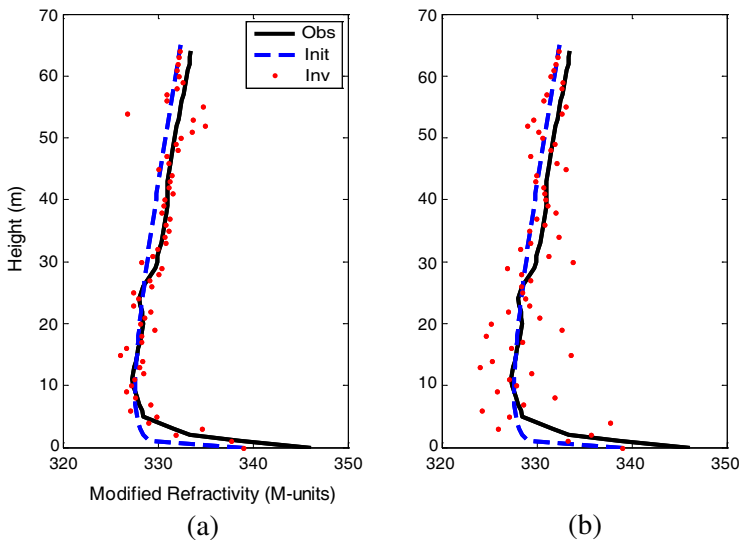


**Figure 9.** Inversions for different Gaussian noise. (a) 10% Gaussian noise. (b) 20% Gaussian noise.

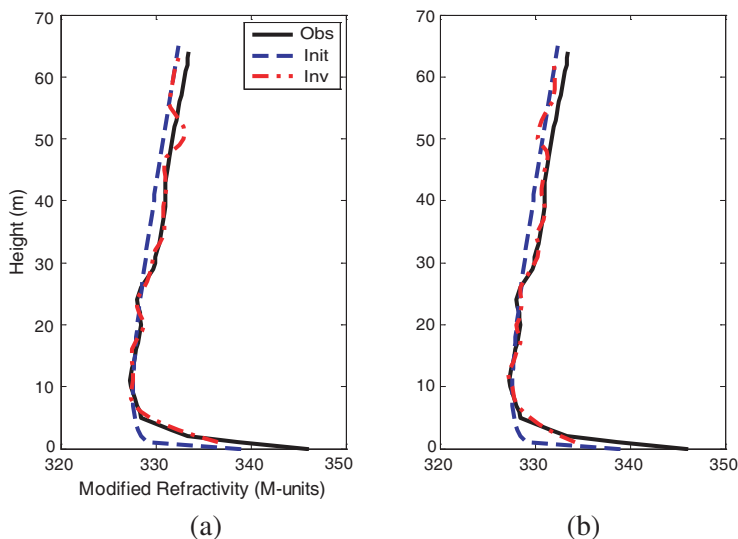


**Figure 10.** The curve fitting results of Fig. 9. (a) 10% Gaussian noise. (b) 20% Gaussian noise.

### 4.3. Influence of the spatial samples

Inversion accuracy of the adjoint approach is dependent on the distributions of the observed data. If the observations are extraordinarily insufficient, it is difficult to obtain qualified retrievals. In the above simulations, the propagation distance is selected as 50 km, and the range increment  $\delta x$  is 20 m. How about other geometries? Fig. 11 gives the retrievals of 50 km propagation distance with 100 m and 500 m range increment for the left and right subplots, respectively. Fig. 12 gives the retrievals of 5 km propagation distance with 10 m and 50 m range increment for the left and right subplots, respectively.

From the above two Figures, it is clear that at a given propagation distance, the inversion accuracy is reducing with the increase of the step range. This is because using the split-step Fourier algorithm to solve the forward and adjoint model, the solutions depend on the step range [24]. Another reason is that it is impossible to obtain the analytical expression of Eq. (30), and the trapezoid formula is adopted to give an approximation to the integral term. The shorter range increment is selected, the more accurate approximation will be obtained. Comparing Fig. 11(a) with Fig. 12(a), even though both geometries have the same spatial samples and the latter has shorter range increment, the performance in Fig. 11(a) is better than that

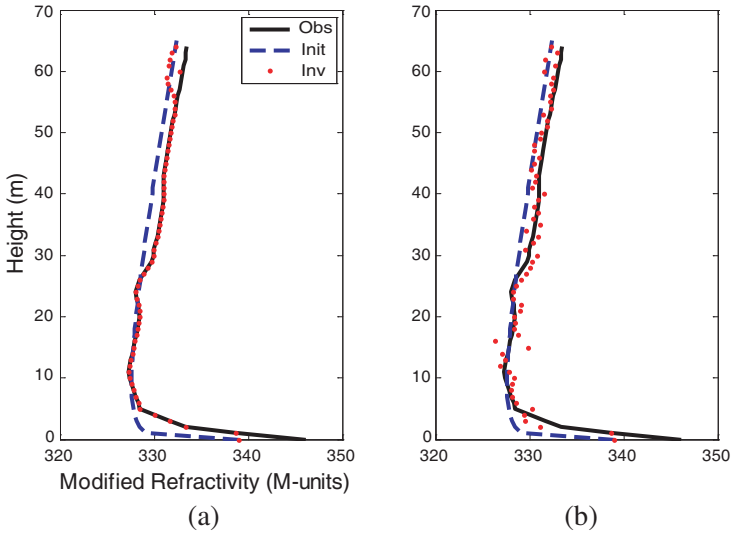


**Figure 11.** Inversions for 50 km propagation distance with different range increment. (a) 100 m range increment. (b) 500 m range increment.

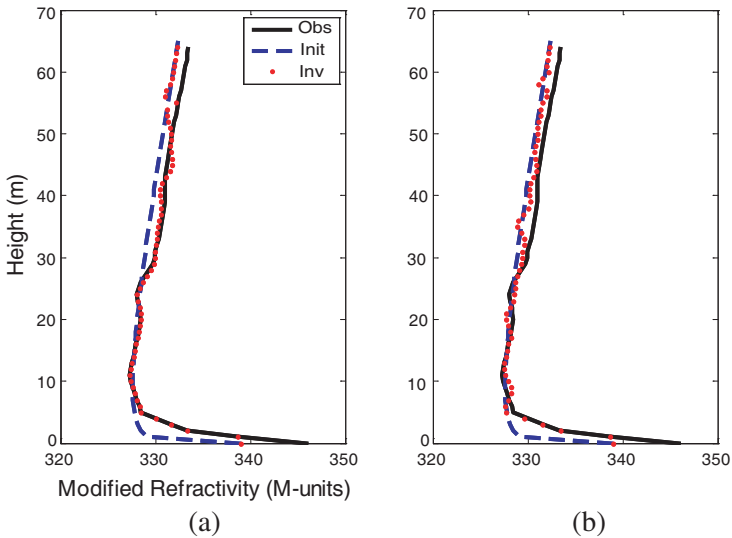


**Figure 12.** Inversions for 5 km propagation distance with different range increment. (a) 10 m range increment. (b) 50 m range increment.

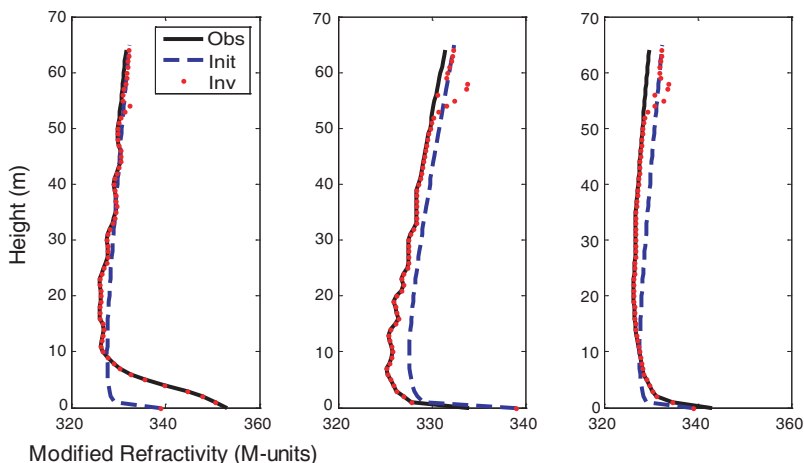


**Figure 13.** Inversions for different duct profiles.

in Fig. 12(a). This phenomenon indicates that extensively spatial sampling could get more signal field characteristics, which is better than the centralized sampling.

The retrievals on a couple of other duct profiles are shown in Fig. 13. The propagation distance is 50 km, the range increment is 100 m, and the maximum iteration number is 400.

## 5. CONCLUSION

The focus of this paper has been on estimating atmospheric refractivity at each point over height from RFC geometry. The detailed derivation of the adjoint model from PE is presented. Numerical simulations are adopted to validate the feasibility of the theoretical algorithm. The performance is evaluated as a function of: 1) the initial guess profile (linear profiles with different  $M$  values at sea surface and Log linear evaporation duct profile); 2) the measurement noise (10% and 20% Gaussian noise); and 3) the spatial samples (50 km propagation distance with 100 m and 500 m range increment, and 5 km propagation distance with 10 m and 50 m range increment). Refractivity profile estimation results are presented for evaporation duct examples collected at East China Sea, which indicate that at a fairish initial guess profile, and the propagation distance and range increment are selected appropriately, the retrieved results can converge to the observed profile with very high accuracy, and the anti-noise ability of the algorithm is favorable.

Through introducing the Delta function into the adjoint model construction, we successfully developed variational adjoint approach for atmospheric refractivity estimations using RFC geometry. Only smooth, perfectly conducting surface and horizontally homogeneous atmospheric conditions were discussed with simulations. Even though promising, these results are preliminary and future work is required to evaluate the performance of the method with real measured data, as well as more complex environment conditions.

## ACKNOWLEDGMENT

The authors would like to thank Professor Gerstoft P. and Yardim C. in Marine Physical Laboratory, University of California, San Diego, for discussions about constructions of cost function. This work is supported by the National Natural Science Foundation of China (Grant No. 40775023).

## REFERENCES

1. Yardim, C., "Statistical estimation and tracking of refractivity from radar clutter," Ph.D. dissertation, Electrical Engineering, University of California, San Diego, 2007.
2. Wang, B., Z. S. Wu, Z. W. Zhao, and H. G. Wang, "Retrieving evaporation duct heights from radar sea clutter using particle swarm optimization (PSO) algorithm," *Progress In Electromagnetics Research M*, Vol. 9, 79–91, 2009.
3. Tabrikian, J., J. L. Krolik, and S. Vasudevan, "Estimating tropospheric refractivity parameters from radar sea clutter," *Proceedings of the IEEE Signal Processing Workshop on Higher-Order Statistics*, 345–348, IEEE Press, Piscataway, New Jersey.
4. Rogers, L. T., C. P. Hattan, and J. K. Stapleton, "Estimating evaporation duct heights from radar sea echo," *Radio Sci.*, Vol. 35, No. 4, 955–966, 2000.
5. Gerstoft, P., L. T. Rogers, J. L. Krolik, and W. S. Hodgkiss, "Inversion for refractivity parameters from radar sea clutter," *Radio Sci.*, Vol. 38, No. 3, 8053, 2003, doi:10.1029/2002RS002640.
6. Gerstoft, P., L. T. Rogers, W. S. Hodgkiss, and L. J. Wagner, "Refractivity estimation using multiple elevation angles," *IEEE J. Oceanic Eng.*, Vol. 28, No. 3, 513–525, 2003.
7. Barrios, A. E., "Estimation of surface-based duct parameters from surface clutter using a ray trace approach," *Radio Sci.*, Vol. 39, RS6013, 2004, doi:10.1029/2003RS002930.

8. Vasudevan, S., R. H. Anderson, S. Kraut, P. Gerstoft, L. T. Rogers, and J. Krolik, "Recursive Bayesian electromagnetic refractivity estimation from radar sea clutter," *Radio Sci.*, Vol. 42, RS2014, 2007, doi:10.1029/2005RS003423.
9. Yardim, C., P. Gerstoft, and W. S. Hodgkiss, "Estimation of radio refractivity from radar clutter using bayesian monte carlo analysis," *IEEE Trans. Antennas Propag.*, Vol. 54, No. 4, 1318–1327, 2006.
10. Yardim, C., P. Gerstoft, and W. S. Hodgkiss, "Statistical maritime radar duct estimation using hybrid genetic algorithm-Markov chain Monte Carlo method," *Radio Sci.*, Vol. 42, RS3014, 2007, doi:10.1029/2006RS003561.
11. Yardim, C., P. Gerstoft, and W. S. Hodgkiss, "Tracking refractivity from clutter using Kalman and particle filters," *IEEE Trans. Antennas Propag.*, Vol. 56, No. 4, 1058–1070, 2008.
12. Douvenot, R., V. Fabbro, P. Gerstoft, C. Bourlier, and J. Saillard, "A duct mapping method using least squares support vector machines," *Radio Sci.*, Vol. 43, RS6005, 2008, doi:10.1029/2008RS003842.
13. Douvenot, R., V. Fabbro, P. Gerstoft, C. Bourlier, and J. Saillard, "Real time refractivity from clutter using a best fit approach improved with physical information," *Radio Sci.*, Vol. 45, RS1007, 2010, doi:10.1029/2009RS004137.
14. Huang, S. X., X. F. Zhao, and Z. Sheng, "Refractivity estimation from radar sea clutter," *Chin. Phys. B*, Vol. 18, No. 11, 5084–5090, 2009.
15. Sheng, Z., S. X. Huang, and X. F. Zhao, "The determination of observation weight in inversion ocean duct using radar clutter," *Acta Phys. Sin.*, Vol. 58, No. 9, 6627–6632, 2009.
16. Zhao, X. F., S. X. Huang, and Z. Sheng, "Ray tracing/correlation approach to estimation of surfaced-based duct parameters from radar clutter," *Chin. Phys. B*, Vol. 19, No. 4, 049201, 2010.
17. Huang, S. X. and R. S. Wu, *Mathematical Physics Problems in Atmospheric Science*, 2nd Edition, Meteorology Press, Beijing, China, 2005.
18. Hursky, P., M. B. Porter, B. D. Cornuelle, W. S. Hodgkiss, and W. A. Kuperman, "Adjoint modeling for acoustic inversion," *J. Acoust. Soc. Am.*, Vol. 115, No. 2, 607–619, 2004.
19. Hermand, J. P., M. Meyer, M. Asch, and M. Berrada, "Adjoint-based acoustic inversion for the physical characterization of a shallow water environment," *J. Acoust. Soc. Am.*, Vol. 119, No. 6,

- 3860–3871, 2006.
20. Zhao, X. F., S. X. Huang, and H. D. Du, “Theoretical analysis and numerical experiments of variational adjoint approach for refractivity estimation,” *Radio Sci.*, Vol. 46, RS1006, 2011, doi:10.1029/2010RS004417.
  21. Dockery, G. D., “Modeling electromagnetic wave propagation in the troposphere using the parabolic equation,” *IEEE Trans. Antennas Propag.*, Vol. 36, No. 10, 1464–1470, 1988.
  22. Barrios, A. E., “Radio wave propagation in horizontally inhomogeneous environments by using the parabolic equation method,” Technical Report, 1430, 1991.
  23. Barrios, A. E., “Parabolic equation modeling in horizontally inhomogeneous environments,” *IEEE Trans. Antennas Propag.*, Vol. 40, No. 7, 791–797, 1992.
  24. Kuttler, J. R. and G. D. Dockery, “Theoretical description of the parabolic approximation/Fourier split-step method of representing electromagnetic propagation in the troposphere,” *Radio Sci.*, Vol. 26, No. 2, 381–393, 1991.
  25. Barrios, A. E., “A terrain parabolic equation model for propagation in the troposphere,” *IEEE Trans. Antennas Propag.*, Vol. 42, No. 1, 90–98, 1994.
  26. Hitney, H. V., J. H. Richter, R. A. Pappert, K. D. Anderson, and G. B. Baumgartner, “Tropospheric radio propagation assessment,” *Proceedings of the IEEE*, Vol. 73, No. 2, 265–285, 1985.
  27. Zhu, C., R. H. Byrd, P. Lu, and J. Nocedal, “L-BFGS-B-Fortran subroutines for large-scale bound constrained optimization,” Northwestern University EECS Technical Report NAM12, 1995.
  28. Harris F. J., “On the use of windows for harmonic analysis with the discrete fourier transform,” *Proceedings of the IEEE*, Vol. 66, No. 1, 51–83, 1978.
  29. Ding, J. L., J. F. Fei, X. G. Huang, X. Zhang, X. Zhou, and B. Tian, “Contrast on occurrence of evaporation ducts in the south china sea and east china sea area,” *Chinese Journal of Radio Science*, Vol. 24, No. 6, 1018–1023, 2009.
  30. Hitney, H. V. and R. Vieth, “Statistical assessment of evaporation duct propagation,” *IEEE Trans. Antennas Propag.*, Vol. 38, No. 6, 794–799, 1990.
  31. Chen, Z. C., *Partial Differential Equation*, 2nd edition, Chinese Science and Technology University Press, Hefei, China, 2002.